JOURNAL OF GEOPHYSICAL RESEARCH, VOL. 113, D18205, doi:10.1029/2007JD009605, 2008



# Orographic cirrus in the global climate model ECHAM5

H. Joos,[1] P. Spichtinger,[1] U. Lohmann,[1] J.-F. Gayet,[2] and A. Minikin[3]

Received 15 November 2007; revised 5 June 2008; accepted 26 June 2008; published 27 September 2008.

[1] A comparison of satellite data with simulations from global circulation models shows that there is a lack of cirrus cloud amount in large-scale models above and in the lee of mountains. The formation of orographic cirrus clouds due to gravity waves is usually not parameterized in large-scale models. To improve the simulation of such orographically excited cirrus clouds a coupling of the gravity wave dynamics and the cloud microphysics has been implemented in the climate model European Centre/Hamburg 5 (ECHAM5). As homogeneous freezing of solution droplets strongly depends on the vertical velocity, an increased vertical velocity due to gravity wave activity in the upper troposphere leads to the formation of cirrus clouds with higher ice crystal number densities. A comparison of the new parameterization with measurements shows a better agreement with observations.

**Citation:** Joos, H., P. Spichtinger, U. Lohmann, J.-F. Gayet, and A. Minikin (2008), Orographic cirrus in the global climate model ECHAM5, *J. Geophys. Res.*, *113*, D18205, doi:10.1029/2007JD009605.

## 1. Introduction

[2] Cirrus clouds play an important role in the climate system. They cover approximately 30% of the Earth and can influence the radiative budget of the Earth in two different ways. Ice crystals scatter part of the incoming solar radiation back to space. This leads to a cooling of the underlying atmosphere (albedo effect of clouds). On the other hand, ice crystals reduce the outgoing longwave radiation and can lead to a warming (greenhouse effect of clouds). Which process is dominant depends on the properties of the cirrus cloud like ice crystal number density, thickness of the cloud, and ice water content. In general it is thought that optically thin cirrus have a warming effect and optically thick cirrus a cooling effect. Thus a net global warming of the Earth-atmosphere system due to cirrus clouds is possible [*Chen et al.*, 2000]. However, an estimate of the global influence of cirrus clouds on the radiative budget is very complex as the formation processes and the life cycle of cirrus clouds are not very well known [*Spichtinger et al.*, 2005a, 2005b] and especially the transition from the cooling to the warming regime is not yet completely understood. Recent studies indicate that the ice crystal number density plays a crucial role for the transition from warming to cooling due to cirrus clouds [*Fusina et al.*, 2007].

[3] Ice crystals form either owing to homogeneous freezing of supercooled solution droplets or owing to heterogeneous nucleation. Thereby homogeneous freezing of droplets of a certain size starts when the relative humidity with respect to ice exceeds a threshold which depends only on the temperature [*Koop et al.*, 2000]. The heterogeneous freezing is initiated by aerosol particles, the so-called ice nuclei. The supersaturation with respect to ice, which is required for heterogeneous freezing depends on the properties of the ice nuclei. In general, the supersaturation threshold for heterogeneous nucleation is lower than for homogeneous freezing [*DeMott et al.*, 2003].

[4] An important factor for triggering the formation of ice is the vertical velocity. It induces adiabatic cooling and thus an increase of the relative humidity with respect to ice. Mesoscale velocity fluctuations in the range of 10–50 cm/s amplify homogeneous nucleation [*Haag and Kärcher*, 2004; *Hoyle et al.*, 2005]. For example, if the vertical velocity increases from 10 to 100 cm/s, the number of newly frozen particles rises more than 1 order of magnitude [*Kärcher and Lohmann*, 2002]. Amongst others, these mesoscale fluctuations in the vertical velocity can be induced by gravity waves. One important source of gravity waves are mountains producing orographic waves. There are lots of mountainous regions in the world, where an influence of the gravity waves on the formation of clouds has to be considered [*Kärcher and Ström*, 2003]. An additional process which contributes to the vertical velocity induced by gravity waves is turbulence created by gravity wave breaking. This process is not yet included in the proposed parameterization. *Dean et al.* [2005] analyzed satellite data from the ISCCP project and compared them with the results of the 19-level HadAM3 version of the United Kingdom Met Office Unified Model. They showed that the model does not simulate sufficient high cloud cover over land especially in the regions of the mountains. Therefore they proposed a parameterization of orographic clouds described by *Dean et al.* [2007].

[5] In this parameterization *Dean et al.* [2007] calculate temperature perturbations due to subgrid-scale orographic gravity waves which can lead to the formation of ice.

[1]Institute for Atmospheric and Climate Science, ETH Zurich, Zurich, Switzerland.
[2]Laboratoire de Meteorologie Physique, Universite Blaise Pascal, Clermont-Ferrand, France.
[3]Institute of Atmospheric Physics, DLR, Oberpfaffenhofen, Germany.


0148-0227/08/2007JD009605$09.00

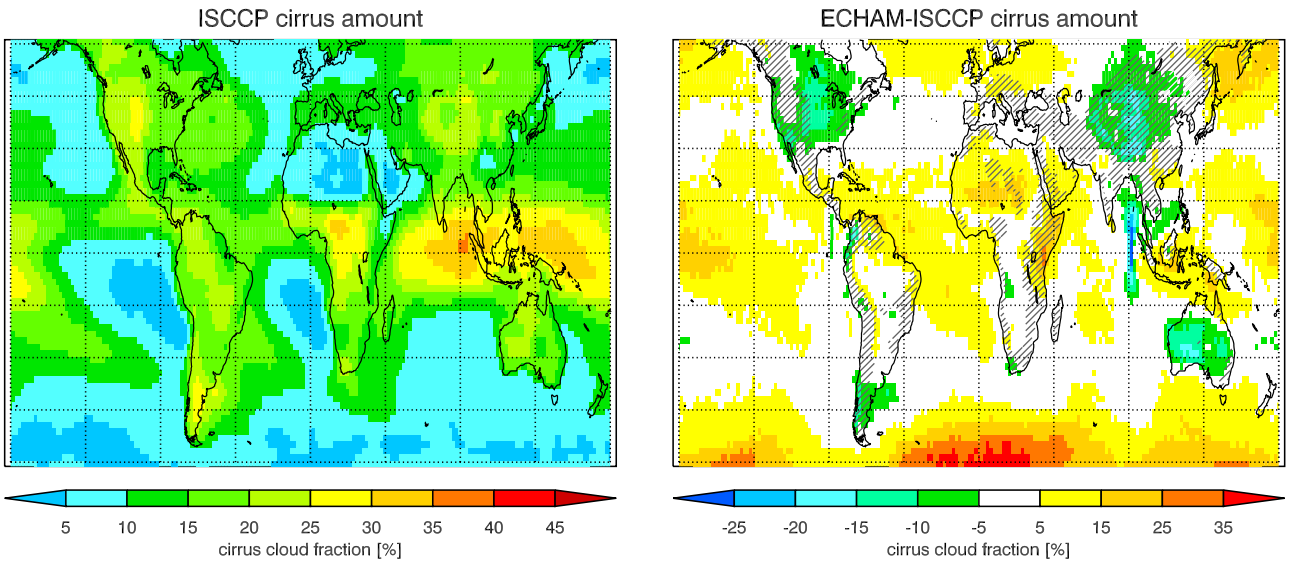


**Figure 1.** (left) Annual mean ISCCP Cirrus cloud amount (percentage of a grid box covered with cirrus) for the years 1983–2005 and (right) the difference between a 3-year ECHAM5 simulation and ISCCP. Cirrus clouds are defined as clouds above 440 hPa and an optical depth $\tau < 3.6$. The grey shaded regions show where the gravity wave scheme can be activated. See also section 3.2.

However, only the ice water content can be influenced with this parameterization. In order to improve the simulation of cirrus clouds and their influence on the radiative budget, it is necessary to include the vertical velocity induced by gravity waves in the calculation of ice crystal formation.

[6] The comparison of the cirrus cloud cover simulated with the European Centre/Hamburg 5 (ECHAM5) global climate Model (GCM) used in this study [*Lohmann et al.*, 2007] with observations from the International Satellite Cloud Climatology Project (ISCCP) [*Rossow and Schiffer*, 1999] also shows a lack of cirrus cloud cover over continents and in the mountainous regions, as shown in Figure 1. The grey shaded regions in Figure 1 (right) show where the gravity wave scheme can be activated. There are some regions where one would expect a more pronounced lack of cirrus cloud amount like the tip of south America. However, in the ISCCP data set only clouds with an optical depth >0.1 are detected. This leads to an underestimation of thin cirrus. Additionally, thin cirrus overlying thicker low-level clouds could be assigned to a wrong cloud class and thus additionally lead to an underestimation of cirrus [*Dean et al.*, 2005]. The cloud amount calculated within the ECHAM5 GCM is based on an ISCCP simulator [*Klein and Jakob*, 1999; *Webb et al.*, 2001] in order to simulate the cloud amount as it is seen by the satellites. However, this cloud amount also includes clouds with optical depth <0.1 for which reason the GCM is expected to see more cirrus as it also includes the optical thin cirrus. Therefore we can conclude that ECHAM underestimates the cirrus cloud cover in many regions where we also can expect gravity wave activity (grey shaded areas) like the southern Andes, the Rocky mountains or the Himalaya. However over Australia the lack of cirrus cannot be caused by a lack of gravity wave activity. The seasonal analysis shows that the cirrus cloud cover is maximal in summer (DJF) possibly caused by weak convection or weak frontal lifting [*Dean et al.*, 2005].

[7] In this paper we therefore present a new concept of coupling the gravity wave dynamics and cloud microphysics in the climate model ECHAM5 [*Roeckner et al.*, 2003]. In our parameterization we explicitly calculate a vertical velocity induced by gravity waves which is used directly in the parameterization of homogeneous freezing. Since a double-moment scheme for the ice phase is implemented in ECHAM5, we are able to influence not only the ice water content but also the ice crystal number concentration.

[8] In section 2, the parameterization of homogeneous freezing in ECHAM5 is described. In section 3 the calculation of a vertical velocity induced by gravity waves and a description of the orography used in ECHAM5 is presented and in section 4 results obtained with the new parameterization are discussed. Additionally a comparison with in situ measurements for a case study is shown. In section 5 we summarize our work and draw some conclusions.

## 2. Parameterization of Cirrus Clouds: Homogeneous Freezing

[9] Homogeneous freezing of supercooled solution droplets plays an important role for the formation of cirrus in the upper troposphere. The lack of efficient ice nuclei, high ice crystal number densities frequently measured in young cirrus clouds and the frequently observed high relative humidities with respect to ice indicate the importance of homogeneous freezing as an important mechanism for the formation of cirrus [*Sassen and Dodd*, 1989]. The formation of gravity waves with high vertical velocities leads to very high supersaturations with respect to ice and one can assume that homogeneous freezing is the dominant freezing mechanism [*Kärcher and Ström*, 2003].

[10] *Kärcher and Lohmann* [2002] developed a parameterization for the formation of cirrus due to homogeneous freezing of supercooled solution droplets. This parameteri-

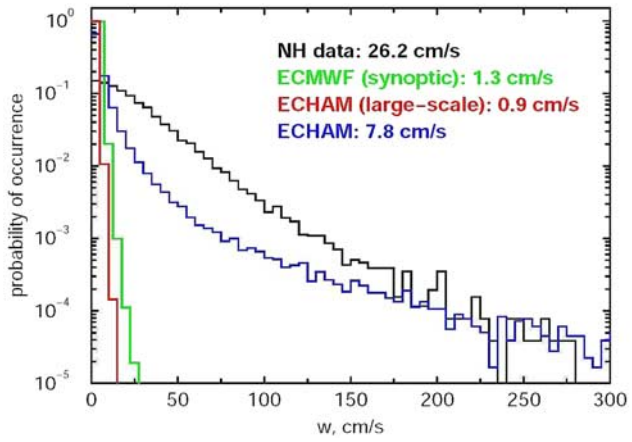


**Figure 2.** Histogram of vertical velocities from the Northern Hemisphere data set from the INCA-campaign, from upper tropospheric synoptic-scale winds calculated by the ECMWF weather forecast model, from upper tropospheric large-scale winds calculated by ECHAM4, and from upper tropospheric winds with a contribution from the turbulent kinetic energy. Numbers in the legend indicate the mean vertical velocities [*Kärcher and Ström*, 2003].

zation is implemented in the version of ECHAM5 used for this study [*Lohmann et al.*, 2007].

[11] The number of newly frozen ice particles depends on a critical ice supersaturation $S_{cr}$, which only depends on temperature [*Koop et al.*, 2000], the water vapor number density at ice saturation $n_{sat}$ and the vertical velocity $w$. Furthermore, the maximal number of newly frozen ice crystals cannot exceed the number of hygroscopic aerosol particles $N_a$. Hence, the number of newly frozen ice crystals due to homogeneous freezing $N_i^{hom}$ is given by

$$N_i^{hom} = \min\left[\frac{m_w}{\rho_i}\left(\frac{b_2}{2\pi b_1}\right)^{3/2}\frac{a_1 S_{cr}}{a_2 + a_3 S_{cr}}\frac{w}{\sqrt{\tau}}; N_a\right], \quad (1)$$

where $m_w$ is the mass of a water molecule, $\rho_i$ is the density of ice (= 925 kg m$^{-3}$), $S_{cr}$ denotes the critical supersaturation where homogeneous freezing starts, $\tau \propto 1/w$ is the characteristic timescale of the nucleation event, $a_1$, $a_3$ and $b_2$ are temperature-dependent variables, $a_2 \propto 1/n_{sat}$ and $b_1 \propto n_{sat}(S_{cr} - 1)$, respectively. For a more detailed explanation see *Kärcher and Lohmann* [2002] and *Lohmann and Kärcher* [2002]. From equation (1) one can deduce the approximate scaling relationship

$$N_i^{hom} \propto w^{3/2} n_{sat}^{-1/2}. \quad (2)$$

[12] The positive correlation between $N_i^{hom}$ and $w$ shows that the number density of freshly formed ice crystals increases with increasing vertical velocity. Higher vertical velocities lead to higher supersaturations allowing more ice crystals to form before the supersaturation is depleted efficiently. At lower temperatures the depositional growth is less efficient, thus the growing ice crystals need longer to take up the available water vapor and to reduce the supersaturation [*Pruppacher and Klett*, 1997]. Therefore, the high supersaturations can exist over a longer time period and more ice crystals can be formed [*Kärcher and Lohmann*, 2002].

[13] So far, the vertical velocity used in this parameterization consists of two parts. A large-scale, grid mean vertical velocity $w_l$ and a contribution from the turbulent kinetic energy (TKE), in order to represent the subgrid-scale variabilities in the vertical velocity. The total vertical velocity used in this parameterization is then given by

$$w_{l+t} = w_l + 0.7\sqrt{\mathrm{TKE}} = w_l + w_t. \quad (3)$$

Figure 2 [*Kärcher and Ström*, 2003] shows a histogram of the vertical velocities in the upper troposphere (175–275 hPa) for four different vertical velocities from observations, the ECMWF model and the former version of the ECHAM model (ECHAM4). By adding a contribution from the TKE to the large-scale vertical velocity, considerably higher vertical velocities can be calculated so that the measured values are reproduced better. Nevertheless, the probability of occurrence of velocities between ~10 cm/s and ~200 cm/s is too small. According to measurements [e.g., *Smith et al.*, 2007] and the (linear) theory of gravity waves [*Smith*, 1979] this is the range where a contribution from non breaking gravity waves can be expected. Thus, an additional vertical velocity induced by orographic gravity waves, as described in the next chapter would lead to an enhanced probability of occurrence in the desired range.

## 3. Calculation of the Vertical Velocity

### 3.1. Linear Theory for Gravity Waves

[14] The calculation of the vertical velocity induced by gravity waves is based on the parameterization of orographic gravity waves from *Lott and Miller* [1997] which is part of the standard ECHAM5 model. Gravity waves can be excited when stably stratified air flows over mountains. Such waves can propagate to considerable altitudes before they dissipate [*McFarlane*, 1987]. An important property of such vertically propagating waves is the transport of momentum from the Earth's surface to the regions where they dissipate. This transport of momentum significantly influences the large-scale circulation in the stratosphere [*McFarlane*, 1987].

[15] In ECHAM5, two mechanisms are considered, which evoke an interaction between the subgrid-scale orography and the atmospheric flow. One mechanism is the transport of momentum from the surface to the atmosphere due to vertically propagating gravity waves, which develop when air flows over mountains. A second considered mechanism is the drag on the flow, which is exerted from the subgrid-scale orography if the flow cannot completely go over the mountain but is blocked at a certain height.

[16] The parameterization of the gravity wave drag is based on the linear theory for monochromatic waves in the hydrostatic regime. As a detailed derivation of the linear theory is beyond the scope of this work, only the main issues are explained here. For more details see, for example, *Smith* [1979]. In order to derive a vertical velocity induced by gravity waves the 2-dimensional equations of motion for an incompressible atmosphere are considered. Additionally

the Boussinesq approximation is used and the Coriolis force is neglected, i.e.,

$$\frac{f}{U} \ll k \ll \frac{N}{U}, \tag{4}$$

where $f$ is the Coriolis parameter, $U$ the horizontal wind speed, $N = \sqrt{g\frac{d\ln\overline{\theta}}{dz}}$ the Brunt-Väisäla frequency and $k = 2\pi/L$ the wave number.

[17] The basic equations for a two-dimensional motion of an incompressible atmosphere are then given by

$$\frac{\partial u}{\partial t} + u\frac{\partial u}{\partial x} + w\frac{\partial u}{\partial z} + \frac{1}{\rho}\frac{\partial p}{\partial x} = 0, \tag{5}$$

$$\frac{\partial w}{\partial t} + u\frac{\partial w}{\partial x} + w\frac{\partial w}{\partial z} + \frac{1}{\rho}\frac{\partial p}{\partial z} + g = 0, \tag{6}$$

$$\frac{\partial u}{\partial x} + \frac{\partial w}{\partial z} = 0, \tag{7}$$

$$\frac{\partial \theta}{\partial t} + u\frac{\partial \theta}{\partial x} + w\frac{\partial \theta}{\partial z} = 0, \tag{8}$$

where $\theta = \frac{p}{\rho R}(\frac{p_s}{p})^{R/cp}$ is the potential temperature, $\rho$ is the density of air, $p$ the pressure, $p_s$ a reference pressure, $R$ the gas constant of air and $c_p$ the heat capacity at constant pressure. Linearizing (5)–(8) about a uniform hydrostatic flow depending only on the altitude for the different variables yields $\rho = \rho_0 + \rho'$, $u = u_0 + u'$, $p = \overline{p}(z) + p'$, $\theta = \overline{\theta}(z) + \theta'$, $w = w'$, $u_0, \rho_0 = const.$ and $\frac{d\overline{p}}{dz} = -\rho_0 g$. After linearizing and some manipulation these equations can be reduced to one equation of the unknown variable $w'$ [see, e.g., *Smith*, 1979],

$$\left(\frac{\partial}{\partial t} + u_0\frac{\partial}{\partial x}\right)^2\left(\frac{\partial^2 w'}{\partial x^2} + \frac{\partial^2 w'}{\partial z^2}\right) + N^2\frac{\partial^2 w'}{\partial x^2} = 0. \tag{9}$$

The solution for vertically propagating waves ($|u_0| < N/k$, where the vertical wave number $m$ is a real number) is given by

$$w' = Re\left(Ae^{i(kx+mz)}\right). \tag{10}$$

The constant $A$ can be determined by the lower boundary condition, namely that the wave is stationary and forced by sinusoidal orography with the height

$$h = h_m \sin(kx), \tag{11}$$

where $h_m$ is the height of the mountain. The linearized lower boundary condition is

$$w|_{z=0} = u_0\frac{\partial h}{\partial x} = u_0 k h_m \cos kx. \tag{12}$$

This leads to the full solution which satisfies equation (9)

$$w' = u_0 k h_m \cos kx \tag{13}$$

and the maximal vertical velocity which is crucial for the initiation of a homogeneous freezing process is given by

$$w' = u_0 k h_m. \tag{14}$$

However, the amplitude of the gravity waves does not only depend on the height of the exciting mountain $h_m$. From the linear theory one also can deduce the vertical displacement of the flow $\delta h$ which depends on the air density $\rho$, the Brunt-Väisäla frequency $N$ and the horizontal wind $u_0$. The change of the amplitude with height can then be calculated as follows:

$$\delta h^2 = \frac{\rho_h N_h U_h h_m^2}{\rho N U} \tag{15}$$

where $\rho_h$, $N_h$, $U_h$ are values averaged between the surface, i.e., the altitude of the resolved orography $Z_{mean}$ and the mountain peak and $\rho$, $N$ and $U$ are values at the considered model level. Here, $U$ is the horizontal wind speed projected in the plane of gravity wave stress at low levels. For a more detailed explanation see, for example, *McFarlane* [1987].

[18] To account for the breaking of gravity waves, an instability criterion based on work by *Lindzen* [1981] is defined: A minimum Richardson number $Ri_{\min}$ that includes the gravity wave influence on the static stability and wind shear is evaluated and given by

$$Ri_{\min} = Ri\frac{1 - (N\delta h/U)}{\left(1 + Ri^{1/2}(N\delta h U)\right)^2}, \tag{16}$$

where $Ri = (N/(dU/dz))^2$ is the background (resolved) flow Richardson number. It is assumed that instability occurs for $Ri_{\min} < 0.25$. This condition takes into account the occurrence of both convective overturning and shear instability. If $Ri_{\min}$ reaches its critical value saturation occurs and the amplitude is restricted to the value at which instability occurs. Thus, $Ri_{\min}$ is set to 0.25 and the saturation amplitude $\delta h_{sat}$ is then calculated using equation (16). Finally we obtained the vertical velocity induced by gravity waves as

$$w_{gw} = k \cdot U \cdot \min(\delta h, \delta h_{sat}) \tag{17}$$

and for the new total vertical velocity we obtain

$$w_{ges} = \underbrace{w_l}_{large-scale} + \underbrace{0.7\sqrt{\mathrm{TKE}}}_{turbulence} + \underbrace{w_{gw}}_{gravity\ waves} = w_l + w_t + w_{gw}. \tag{18}$$

The calculation of the vertical velocity contains a horizontal wave number $k$ which describes the width of the mountain. In the following section it is explained how the subgrid-scale orography in ECHAM5 is represented and which wave numbers, respectively, wavelengths are excited if orographic gravity waves develop.

### 3.2. Orography in ECHAM5

[19] In ECHAM5 the orography is represented as elliptical mountains [*Baines and Palmer*, 1990; *Lott and Miller*,

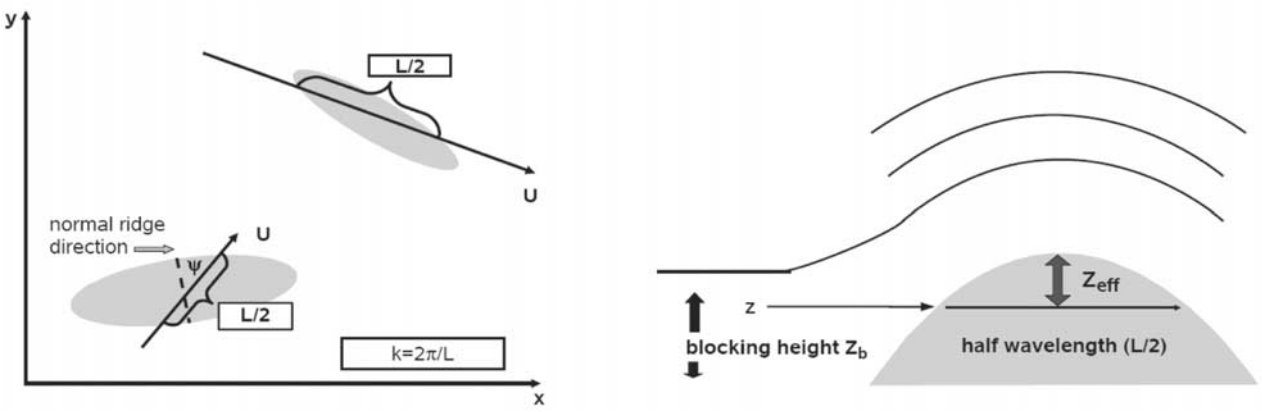


**Figure 3.** Schematic picture of the subgrid-scale orography in ECHAM5. (left) Mountains are described as ellipses which have different orientations in the coordinate system depending on the orientation of the mountains in nature. The excited wavelength $L$ differs depending on the orientation of the mountain and the wind direction (black arrows). (right) Cross section through a mountain. If there is flow blocking, the height of the mountain $h_m$ seen by the flow is reduced to $Z_{eff}$ and the excited wavelength also decreases.

1997]. The anisotropy $\gamma$ of the ellipse is determined by the parameters $a$ and $b$, such that $\gamma = a/b \leq 1$. Then the geometry of the mountain can be written in the form

$$h(x,y) = \frac{H}{1 + x^2/a^2 + y^2/b^2}, \tag{19}$$

i.e., as a bell shaped mountain, where $H$ is the maximum height of the mountain. Furthermore, the subgrid-scale orography (SSO) is represented by the parameters $\mu$, $\sigma$ and $\theta$ which stand for the standard deviation, the slope and the geographical orientation of the orography, respectively, whereas the standard deviation $\mu$ denotes the deviation of the height $h(x, y)$ from the mean (resolved) orography within the area represented by the grid point, as given by the US Navy ($10' \times 10'$) data set as described by *Wallace et al.* [1983]. With these parameters, the grid points where the gravity wave scheme can be activated and gravity waves are excited can be calculated as follows: The difference between the peak height $Z_{\max}$ of the SSO and the mean orography $Z_{mean}$ has to exceed a certain threshold $h_t$ ($Z_{\max} - Z_{mean} > h_t$) and the standard deviation $\mu$ needs to exceed a threshold value $\mu_t$ ($\mu > \mu_t$). The thresholds depend on the model resolution. The higher the resolution, the lower the thresholds. For the resolution of T63 used in this study the thresholds are: $h_t$ = 300 m and $\mu_t$ = 75 m. The areas where this conditions are fulfilled and which represent potential formation regions of gravity waves are shown in Figure 1 (grey shaded regions). However, gravity waves do not develop necessarily at every time step. It also depends on the angle between the orography and the low-level wind if gravity waves are excited or not.

[20] The wavelength of the excited wave $L$ if air flows over this mountain depends on the angle $\psi$ between the incident flow and the normal ridge direction. Additionally, flow blocking is considered, which leads to a reduction of the excited wavelength and the height of the mountain as seen by the flow. Flow blocking occurs, when the nondimensional mountain height $H_n = \frac{NH}{U}$ exceeds 0.5. Figure 3 shows a schematic of the orography in ECHAM5. Figure 3 (left) shows two different mountains with different geographical orientations and anisotropy. The length $l(z)$ that is seen by the incident flow and which corresponds to the half wavelength of the gravity wave depends on the wind direction and is shown here with black arrows. Figure 3 (right) shows a cross section of the mountain. If there is flow blocking, the height of the mountain $h_m$ which excites gravity waves is reduced to $Z_{eff}$ and the length $l(z)$ seen by the flow and thus the wavelength $L$ is reduced as well. To calculate the reduced wavelength in a blocked-flow regime and the reduced effective mountain height $Z_{eff}$ the height of the blocked flow $Z_b$ has to be calculated. It is defined as the lowest level between $Z_{\max}$ and $Z_{\min}$ that satisfies the condition

$$\int_{Z_b}^{Z_{\max}} \frac{N}{U} dz \leq H_{nc} = 0.5, \tag{20}$$

where $H_{nc}$ is a critical nondimensional mountain height which is set to 0.5. Thus, $Z_{eff}$ can be calculated as

$$Z_{eff} = \min\left(H_{nc} \cdot \frac{U}{N}, Z_{\max} - Z_{\min}\right). \tag{21}$$

Hence, if there is no flow blocking, $Z_{eff}$ takes its maximal value and is reduced when flow blocking occurs. For a more detailed description, see *Lott and Miller* [1997].

[21] The length that is seen by the incident flow at a given altitude $z < Z_b$ can be written as

$$l(z) \approx 2\max(a\cos\psi, b\sin\psi)\left(\frac{Z_b - z}{z + \mu}\right)^{1/2}, \tag{22}$$

where $l(z)$ corresponds to the half wavelength $L$. As we are interested in the smallest possible $l(z)$, here $z$ denotes the level just below the level which describes the blocking height $Z_b$. If there is no flow blocking the last term in brackets in equation (22) is set to one and $l(z)$ only depends

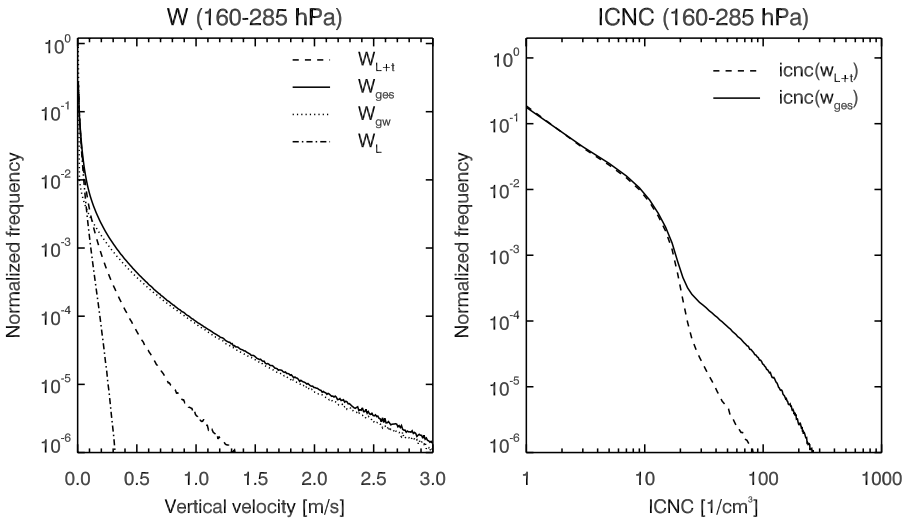


**Figure 4.** (left) vertical velocities (m/s) and (right) ice crystal number concentration ($cm^{-3}$) averaged over the whole globe and the upper troposphere from 165 to 285 hPa; $w_l$ denotes the synoptic-scale vertical velocities, $w_{gw}$ is the vertical velocity induced by gravity waves, $w$ is the synoptic-scale part plus a contribution from the TKE, and $w_{ges}$ is the new total vertical velocity.

on the angle between the incident flow and the SSO. The wave number $k$ used in the calculation of the gravity wave induced vertical velocity is given by $k = 2\pi/(2 \cdot l(z))$.

## 4. Results

[22] In order to investigate the influence of gravity waves on the formation of cirrus clouds simulations with the ECHAM5 GCM [*Roeckner et al.*, 2003] were carried out. We used a horizontal resolution of T63 (1.875° × 1.875°) and 31 vertical levels using a time step of 12 min. The simulations were run for 3 years after a spinup time of 3 months. Climatological sea surface temperature and sea-ice extent with a reference period from January 1979 to February 1996 were used. One reference run (REF) was performed, where the previous vertical velocity described by equation (3) is used. In a second simulation (GWD) the original vertical velocity is replaced by the vertical velocity that contains a contribution from the gravity waves and is described by equation (18).

[23] Additionally, a nudged simulation was performed in order to compare the simulation to observations from the INCA (Interhemispheric differences in cirrus properties from anthropogenic emissions) campaign [*Gayet et al.*, 2004], which took place during March/April 2000 at Punta Arenas, Chile. Nudging is a special assimilation technique where the dynamical model variables are relaxed to observations or meteorological analysis [*Davies*, 1976]. The advantage of a nudged simulation is that the dynamics in the model can be pushed toward observations so that a comparison of certain episodes or measurement campaigns is possible [*Kuo and Guo*, 1989]. For this study the reanalysis data from the ERA40 project [*Uppala et al.*, 2005] at ECMWF (European Centre for Medium-Range Weather Forecasts) were used as observations. In the model, the relaxation timescales for the divergence is 48 hours, for the vorticity 6 hours and for the temperature and surface pressure 24 hours [*Jeuken et al.*, 1996].

### 4.1. Global Simulation

[24] As already mentioned in Figure 2 the probability of occurrence for vertical velocities in the range 10–200 cm/s is too small in the simulations considered. Despite the additional term that contains a contribution from the TKE, vertical velocities in the above mentioned range are generated with a too low frequency. Figure 4 shows the probability of occurrence of the vertical velocity induced by gravity waves ($w_{gw}$), the large-scale vertical velocity ($w_l$), the vertical velocity used in the reference run ($w_{l+t}$) and the new total vertical velocity ($w_{ges}$) for the upper troposphere from 160 to 285 hPa. By employing the gravity wave dynamics a contribution to the vertical velocity develops mainly in the range from 20 to 200 cm/s. This is exactly the range where the probability of occurrence was too low. Adding a vertical velocity induced by gravity waves thus leads to a more realistic distribution of the vertical velocities in the upper troposphere. The changes in the vertical velocity also influence the probability of occurrence of the ice crystal number concentration (ICNC). The ICNC values shown here are only sampled over the cloudy part of the grid box whenever clouds occur. As the cloud fraction is not influenced by the new parameterization, the change in ICNC in the two different simulations is caused only by higher vertical velocities. As a result of the low vertical velocities in the REF simulation, only low ice crystal number densities can be produced. If a contribution from gravity waves is added, higher ICNC can develop and the probability of occurrence in the range of 10–200 $cm^{-3}$ increases considerably. Figure 5 shows a 3-year mean of the vertical velocities and the ice crystal number density for the REF and GWD simulation averaged over the upper troposphere from 165 to 285 hPa. In the REF simulation very low values for the vertical velocity are simulated with maxima up to 20 cm/s in the tropics. In the GWD simulation one can see a completely different distribution of the vertical velocities. There are high values in the range of 5 cm/s to 100 cm/s over the mountains where gravity waves can be excited.

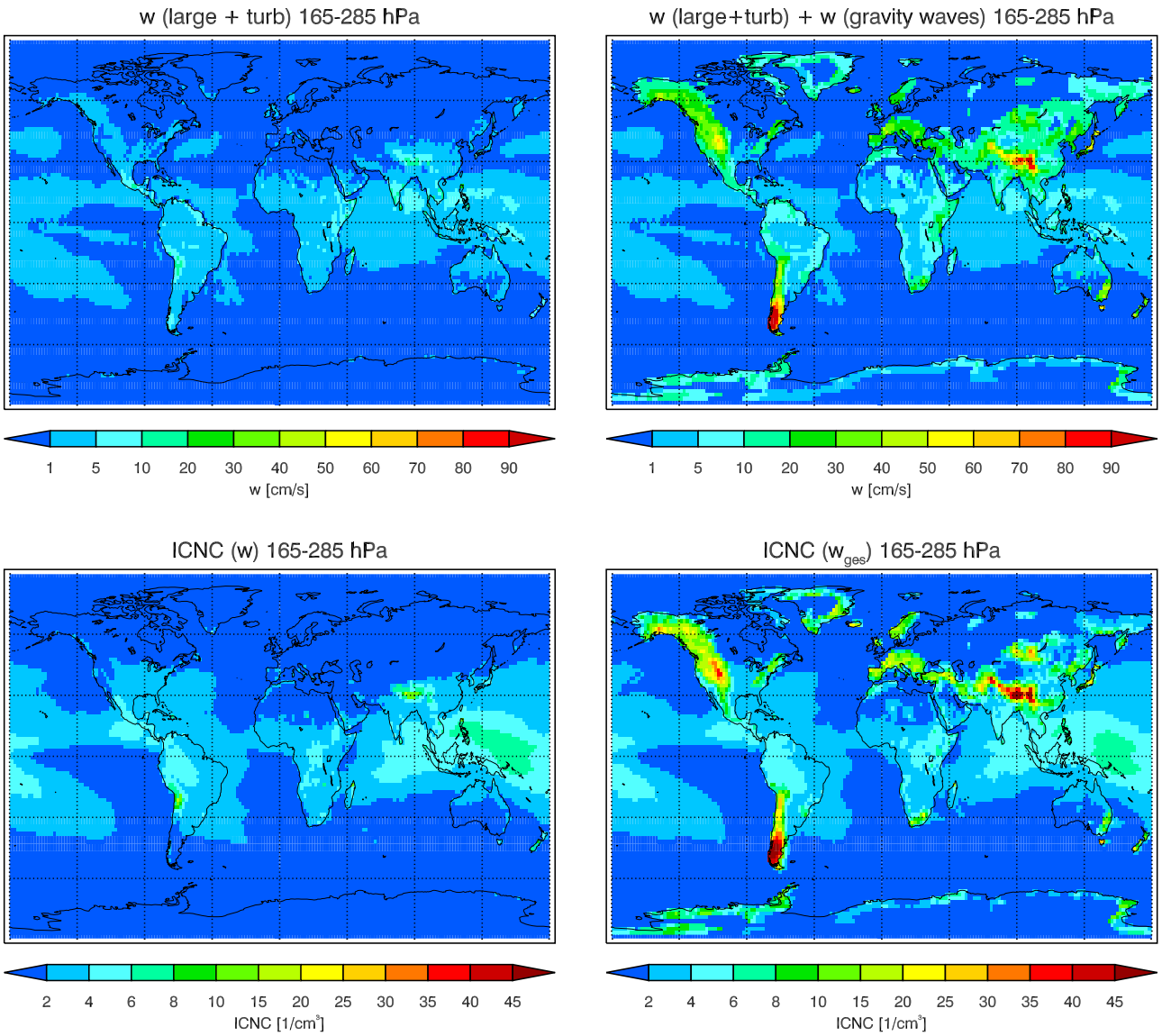


**Figure 5.** (top) Global distribution of the annual mean vertical velocity (cm/s) and (bottom) annual mean of in cloud ice crystal number concentration ($cm^{-3}$) in the upper troposphere (165–285 hPa) for (left) the REF simulation and (right) the GWD simulation.

This leads to a completely new distribution of the vertical wind field which also influences the ice crystal number concentration. The ice crystal number concentration in the REF simulation lies between 1 and 6 $cm^{-3}$. Only in the tropics values of up to 15 $cm^{-3}$ occur owing to convection. There is a lack of ice crystals over continents in general and especially over mountains where we would expect high values due to orographic forcing. In the GWD simulation the model produces much higher concentrations due to the higher vertical velocities. Thus, ice crystals form over the mountains and the ice crystal number concentrations lie between 1 and 5 $cm^{-3}$ over the oceans and up to 40 $cm^{-3}$ over the mountains. Owing to the development of orographic cirrus we can expect a higher cirrus cloud amount in this region and the lack of cirrus clouds over continents can be reduced. Furthermore we see slight advection of ice crystals formed in orographic waves downstream for example to the adjacent ocean at the tip of south America.

### 4.2. Comparison With Measurements

[25] In order to test the new parameterization, the results of the nudged simulation are compared with an orographic cirrus cloud measured during the INCA campaign. The INCA campaign took place in April 2000 in Punta Arenas, Chile and in October 2000 in Prestwick, Scotland. INCA was an aircraft field experiment with the DLR (German Aerospace Center) Falcon aircraft. The measurements used for this comparison were taken at 5 April 2000, between 1700 and 1930 UTC over Chile. Vertical velocities were measured with a five-hole probe [*Bögel and Baumann*, 1991] only during constant altitude flight sections. The accuracy of the vertical velocity is estimated to be on the order of 0.1 m/s. Ice particle concentrations were measured

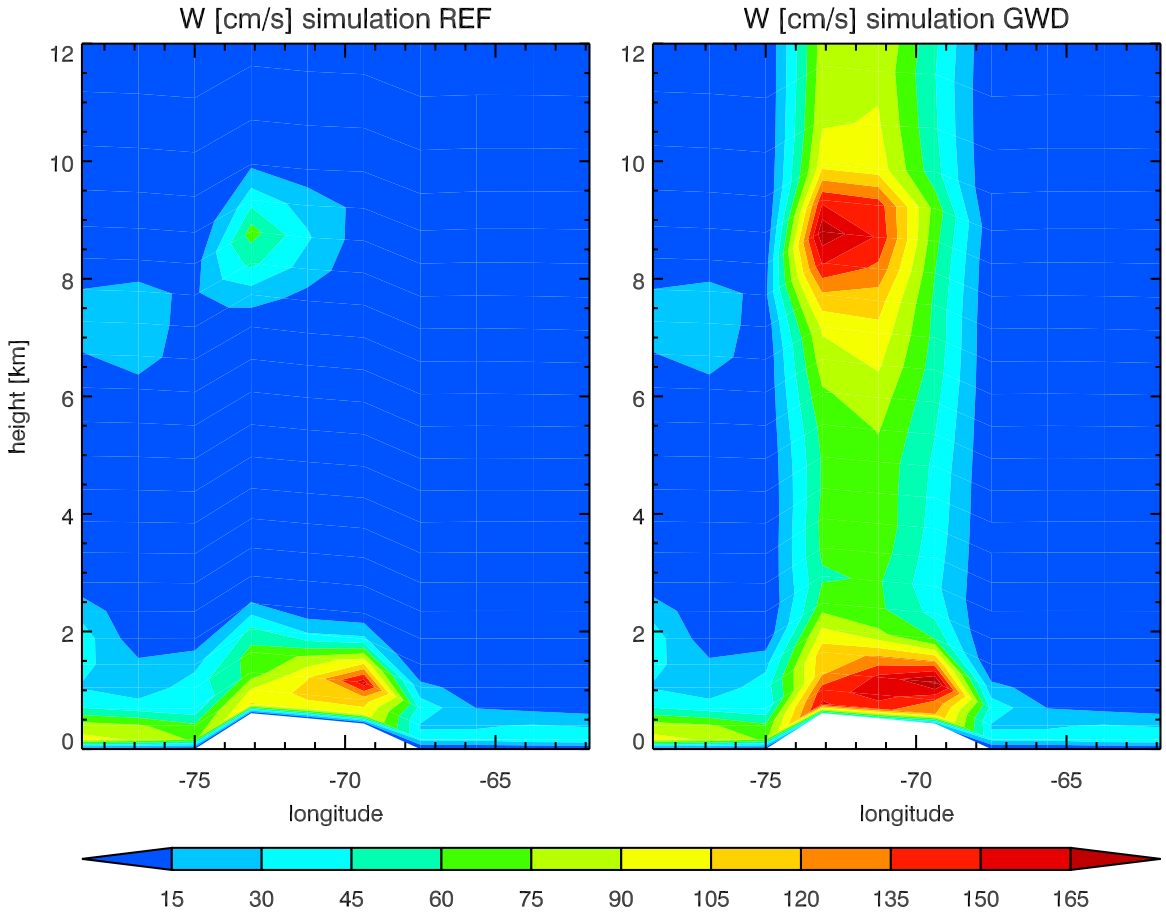


**Figure 6.** Vertical velocity w (cm/s) at a meridional cut over the Andes from 79°W–62°W and 53°S. (left) REF simulation and (right) GWD simulation. Shown is a mean over 17, 18, 19, and 20 UTC, whereas every time step includes a mean over the previous hour. The height of the mountain corresponds to the effective height $Z_{eff}$ which is seen by the incident flow.

during INCA with a combination of two instruments, the FSSP-300 and 2D-C optical probes [*Gayet et al.*, 2002, 2004]. The particle concentrations used for this comparison refer to the particle size range 3–800 micrometer in diameter. As a nudged simulation is used, one can assume that the large-scale flow in the model is similar to the observed one during the measurement day; thus, it makes sense to compare the simulated values with the measured ones. Figure 6 shows the simulated vertical velocities in the troposphere for the nudged REF and GWD simulation. The plots show a meridional cut from 79°W to 62°W at 53°S, which corresponds to the flight track of the measurement airplane. In the REF simulation the vertical velocities in the whole troposphere are very low. Only in the boundary layer higher values can be reached owing to a contribution from the TKE. The contribution from the TKE to the vertical velocity in the upper troposphere is much lower and particularly restricted to a small region. High vertical velocities over mountainous regions due to gravity waves cannot be reproduced accurately by adding a contribution from the TKE to the large-scale vertical velocity. On the contrary, in the GWD simulation a gravity wave is developing, which leads to much higher values of the vertical velocity. The new parameterization thus leads to a different distribution with higher vertical velocities in the whole troposphere which captures the high vertical velocities often observed over mountains. As the parameterization of the ice crystal number density depends strongly on the vertical velocity, the formation of cirrus is also influenced. Figure 7 shows the simulated ice crystal number density for both simulations. The high vertical velocities in the upper troposphere in the GWD simulation lead to the formation of a cirrus cloud in 10 km height with much more ice crystals as in the REF simulation.

[26] In order to compare the in situ measurements with the simulations, the measured values are averaged over a grid box with a horizontal extension of approximately 120 km. For the calculation of the grid mean vertical velocity only the positive velocities are taken as the model only calculates positive subgrid-scale vertical velocities, which are responsible for the initiation of a freezing event. Figure 8 shows the comparison of the measurements and the nudged simulation. As the measurements were taken between 1730 and 1930, the model results shown here are for the output intervals at 1700 UTC, 1800 UTC, 1900 UTC and 2000 UTC. These values are averages over the previous hour.

[27] The GWD simulation can reproduce the large values that have been observed. The previously used vertical velocity (blue) cannot reproduce the high values developing

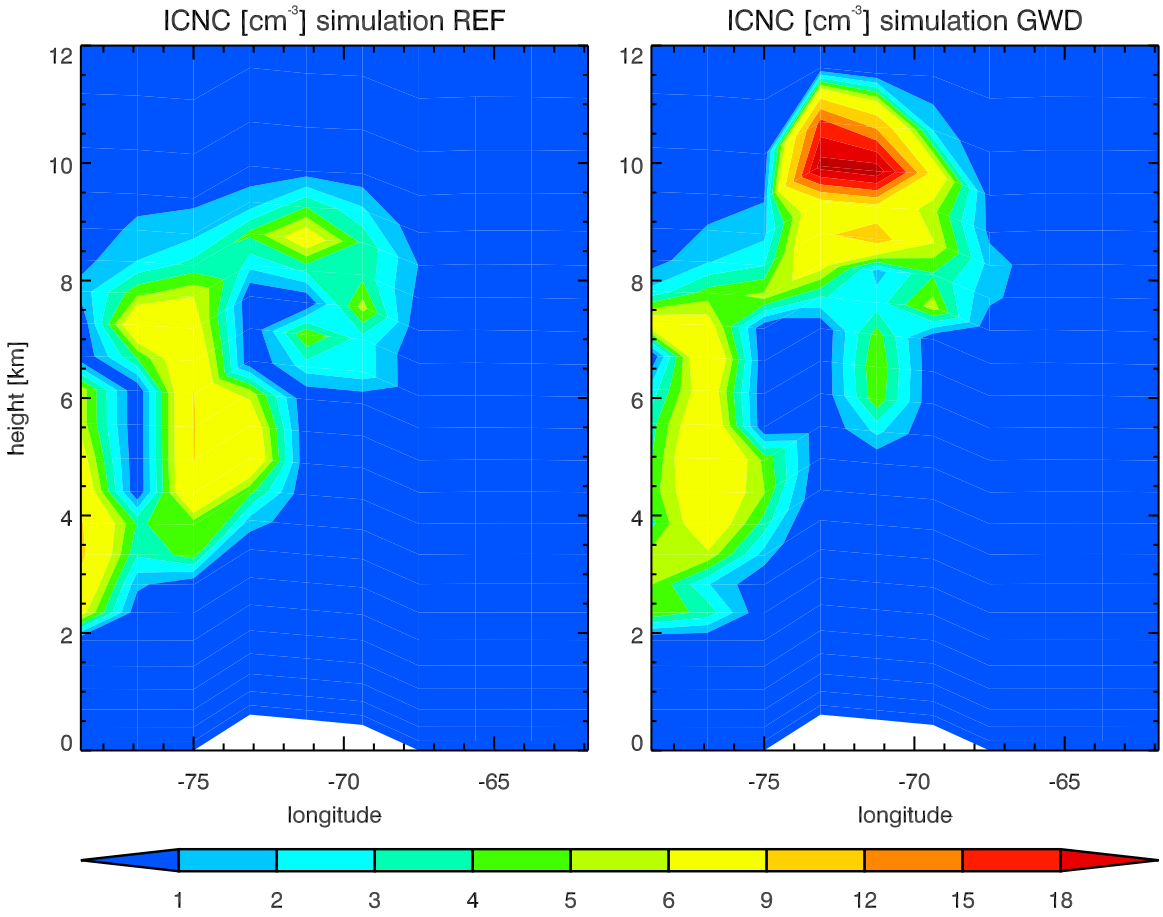


**Figure 7.** Ice crystal number concentration ($cm^{-3}$) at a meridional cut over the Andes from 79°W–62°W and 53°S. (left) REF simulation and (right) GWD simulation. Shown is a mean over 17, 18, 19, and 20 UTC, whereas every time step includes a mean over the previous hour. The height of the mountain corresponds to the effective height $Z_{eff}$ which is seen by the incident flow.

in a gravity wave because it calculates a mean vertical velocity. The new parameterization, on the contrary, calculates a maximum vertical velocity. This maximum vertical velocity is crucial for the onset of homogeneous freezing [*Hoyle et al.*, 2005] and thus more appropriate for the use in the homogeneous freezing parameterization. Furthermore high vertical velocities can be calculated over the whole mountain range and occur not only at one or two grid points as in the old scheme.

[28] The comparison of the measured and simulated ice crystal number concentrations (ICNC) show that the underestimation of the vertical velocities in the REF simulation leads to too low ICNC. The physical process of a developing gravity wave and thus an orographic cirrus cloud is much better represented in the new simulation causing the cloud to form at the correct geographical position. However it seems that the vertical velocity and hence ICNC are slightly overestimated. This could be due to the fact that the vertical velocity contains a contribution from the TKE of up to 30 cm/s which is not physically reasonable. Therefore an additional simulation has been performed, where the contribution from the TKE to the vertical velocity $w_t$ is not taken into account. These results show a better agreement with the observation as the vertical velocity and hence the ICNC slightly decreased (Figure 8, bottom). In future, we will thus neglect or at least decrease the contribution of the TKE to the vertical velocity in areas where gravity waves dominate.

[29] For comparison of the histograms of the vertical velocity and ICNC all values at altitudes higher than 280 hPa and temperatures less than 235 K measured during the southern and northern hemispheric campaign in the area of the measurements were taken. The experimental data represent about 40 flight hours taken during a 4-week period, in each hemisphere. Although these data do not represent climatological averages, their probability frequency distributions should be representative for this region and season and thus can be compared to the results from a nudged simulation. The two regions where measurements were taken are shown in Figure 9. The grey shaded areas in the map show the points where the gravity wave scheme in the model can be activated. In the Northern Hemisphere there are only three grid points where the scheme can become activated and where gravity waves can develop. In the Southern Hemisphere there are nine active points. The histograms for the simulated values are calculated using data from a nudged simulation from March to May 2000 for the southern hemispheric case and from September to November 2000 for the northern hemispheric case for the upper troposphere from 165 to 285 hPa in the measurement

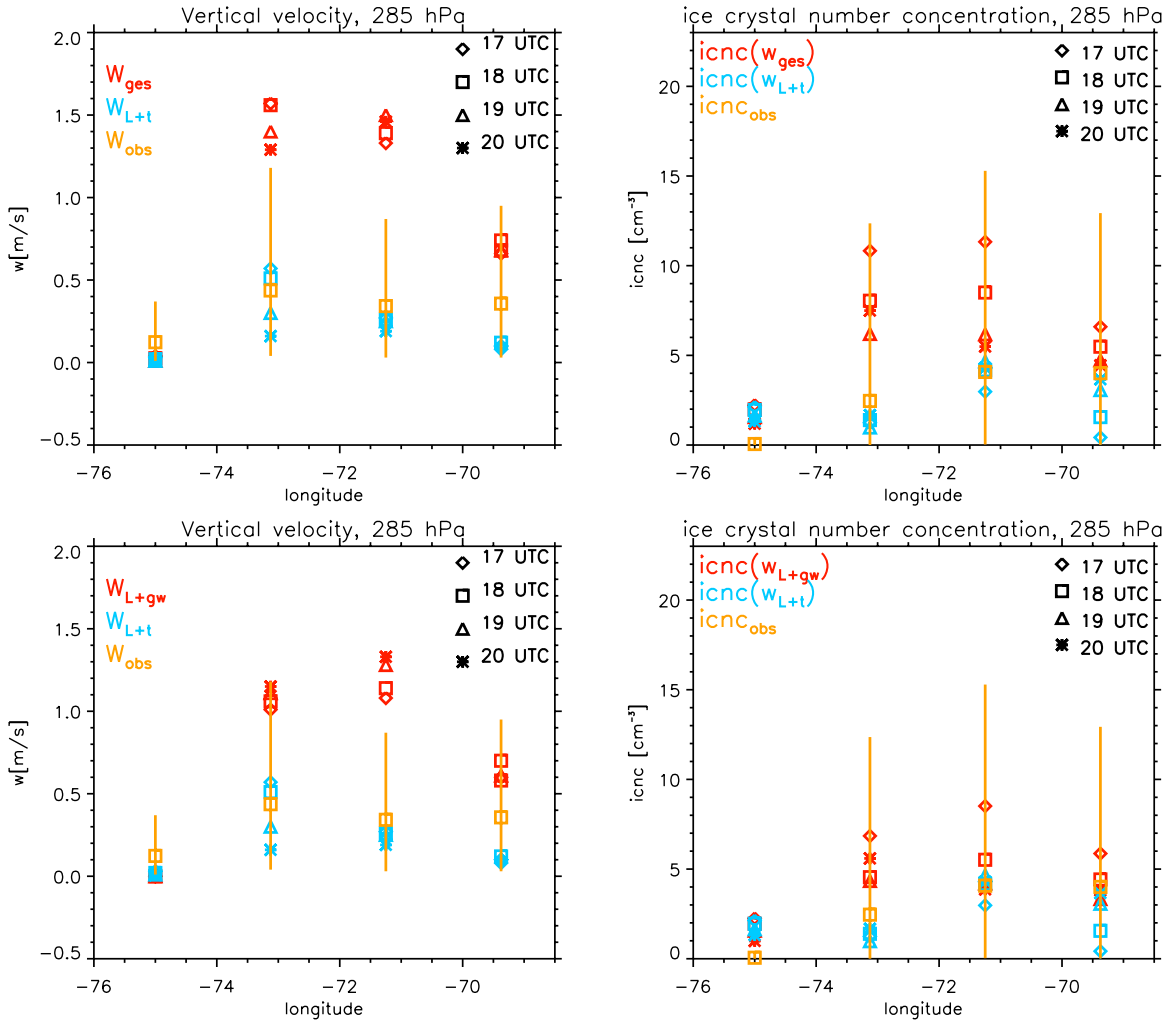


**Figure 8.** Comparison of (left) the simulated vertical velocity and (right) ice crystal number concentration and the measured values from the INCA campaign for four different output intervals and the measurements (orange) taken at 5 April 2000 between 1700 and 1930 UTC at 53°S. The squares denote the mean over the grid box, and the lines denote the 5–95% percentiles. (top) Results for the GWD and REF simulations and (bottom) results for a simulation where the contribution from the TKE to the vertical velocity ($w_t$) is omitted; the vertical velocity is calculated as $w_{ges} = w_l + w_{gw}$.

regions. Figure 10 shows the comparison of the histogram for the measured and simulated values. For the northern hemispheric case one can see that the addition of a gravity wave induced vertical velocity leads to a better representation of the measured values. The values in the range of 0.2 to 2 m/s are shifted to a higher probability of occurrence but cannot reach the measured distribution. This could be due to the fact that in the measurement region there are only three grid points where the gravity wave scheme can be active and thus gravity waves can develop. As the new vertical velocity represents the maximum vertical velocity occurring in a gravity wave but the measurements sample all occurring velocities we expect our new velocities to lie in the upper range of the measurements. We also should mention here that the development of turbulence in breaking gravity waves would lead to an additional vertical velocity which is not yet calculated. This lack of turbulence could lead to an underestimation of the probability of occurrence especially in the range of 10–100 cm/s [*Dörnbrack*, 1998; *Spichtinger and Smolarkiewicz*, 2008]. Using the new parameterization a higher probability of occurrence for the ice crystal number concentration in the range of 10 to 200 $cm^{-3}$ can be simulated which is a better representation of the measured values. For the southern hemispheric case we also obtain an improvement due to the new parameterization. Gravity waves lead to enhanced vertical velocities which better represent the measurements especially in the range of 1 to 2 m/s. Again we expect the simulated values to contribute mainly to the maximum vertical velocities. In this case an additional vertical velocity from turbulence also would enhance the probability of occurrence in the range of 10–100 cm/s. Higher ice crystal number concentrations are also simulated in better agreement with measurements.

## 5. Summary and Discussion

[30] A coupling of gravity wave dynamics and cloud microphysics has been implemented in ECHAM5 in order

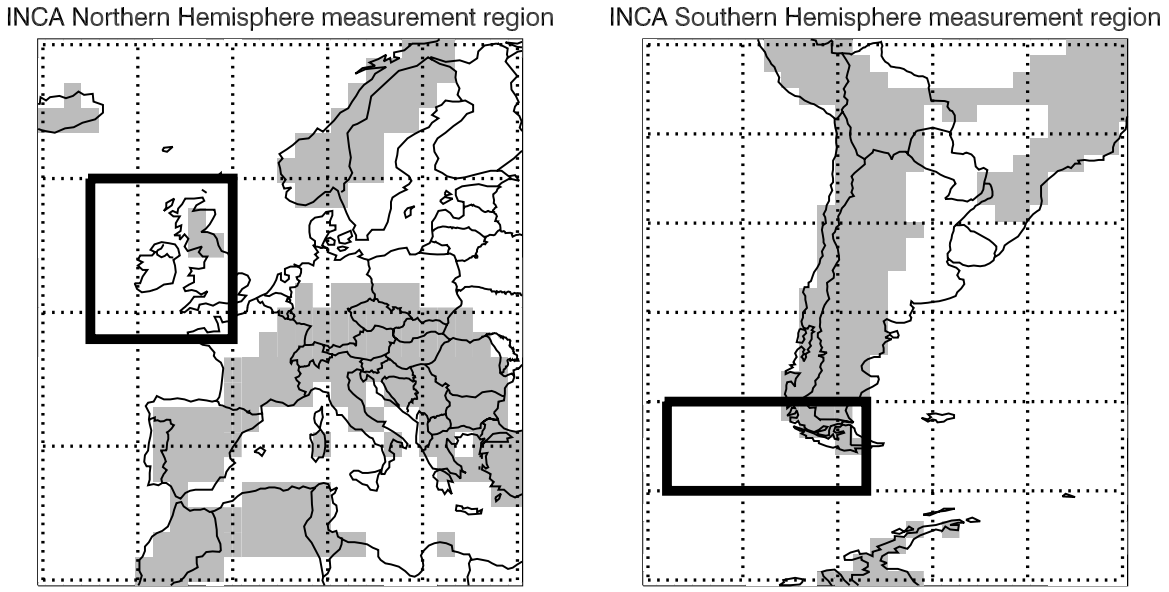


**Figure 9.** Measurement region of the INCA campaign in the Northern and Southern Hemispheres. Grey shaded areas denote grid points where the gravity wave scheme can be activated.

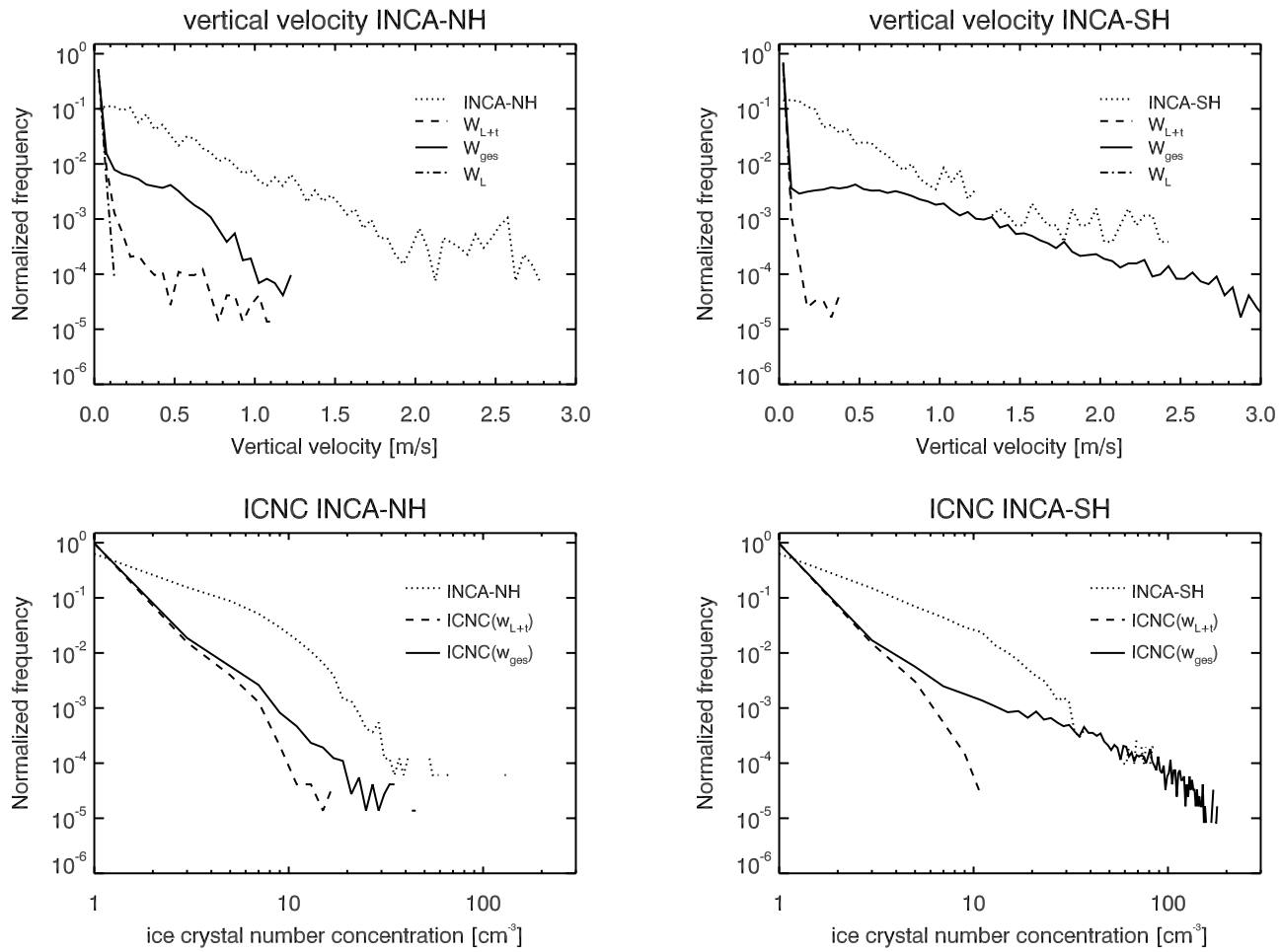


**Figure 10.** Histogram of (top) the measured and simulated vertical velocities (m/s) and (bottom) ice crystal number concentration ($cm^{-3}$) sampled over the measurement regions in (left) the Northern Hemisphere and (right) the Southern Hemisphere shown in Figure 9.

to simulate sufficient amount of cirrus clouds in the lee of mountains. To account for the effect of gravity waves and to simulate the formation process of orographic cirrus an additional component for the vertical velocity has been added to the previously used formula in ECHAM5, which only contains a large-scale part and a contribution from the TKE. The calculation of the vertical velocity induced by gravity waves is based on the parameterization of the gravity wave drag which calculates the momentum transfer from the earth surface to the atmosphere. The contribution of the vertical velocity from gravity waves leads to a much more realistic simulation of the vertical wind field. The probability of occurrence of the vertical velocity in the upper troposphere is enhanced in the range of 20–200 cm/s. This is exactly the range where a contribution due to gravity waves was expected. Good agreement with the measurements from the INCA campaign can be achieved in a direct comparison. Owing to the new parameterization, the annual mean vertically integrated ice crystal number concentration could be enhanced from $1.5 \times 10^{10}$ m$^{-2}$ to $1.67 \times 10^{10}$ m$^{-2}$ which corresponds to an increase of ~11%. Higher ice crystal number concentrations are simulated especially over mountains, which decreases the lack of cirrus over mountains.

[31] Indeed, the new parameterization has a few limitations which should be mentioned here. Currently, the influence of the downdraft of a gravity wave on an orographic cirrus cloud is neglected. As the horizontal extension of an orographic cirrus cloud is limited by strong downdrafts, this limitation of the parameterization should be taken into account in a next step. Moreover, it has to be clarified whether the calculation of the vertical velocity based on a two-dimensional gravity wave scheme has to be modified as the vertical velocities seem to be slightly overestimated (see Figure 8) and the two-dimensional theory leads to an overestimation of the vertical velocities [*Dörnbrack*, 1998]. Additionally, it should be investigated if the contribution from the TKE to the vertical velocity can be dropped or decreased whenever gravity waves occur.

[32] The new distribution of the vertical velocity in the troposphere could also influence the formation of warm and mixed phase clouds via the activation of aerosols into cloud droplets. Thus, the calculation of a more realistic vertical wind field could therefore be of great importance for cloud processes in general.

[33] **Acknowledgments.** We thank Marco Giorgetta, Andrew Orr, Johannes Quaas, and two anonymous reviewers for helpful discussions and suggestions. Furthermore, we thank the Deutsches Klimarechenzentrum (DKRZ) for computing time. This work contributes to the TH-project "Orographic cirrus clouds in the climate model ECHAM5" (grant TH-18 06-1) supported by ETH Research Funds.

## References

Baines, P., and T. Palmer (1990), Rationale of a new physically based parameterization of sub-grid scalep orographic effects, *Tech. Rep. 169*, Eur. Cent. for Medium-Range Weather Forecasts, Reading, U.K.

Bögel, W., and R. Baumann (1991), Test and calibration of the DLR Falcon wind measuring system by maneuvers, *J. Atmos. Oceanic Technol.*, *8*(1), 5–18.

Chen, T., W. Rossow, and Y. Zhang (2000), Radiative effects of cloud-type variations, *J. Clim.*, *13*, 264–286.

Davies, H. (1976), A lateral boundary formulation for multi-level prediction models, *Q. J. R. Meteorol. Soc.*, *102*, 405–418.

Dean, S., B. Lawrence, R. Grainger, and D. Heuff (2005), Orographic cloud in a GCM: The missing cirrus, *Clim. Dyn.*, *24*, 771–780.

Dean, S., J. Flowerdew, B. Lawrence, and S. Eckermann (2007), Parameterisation of orographic cloud dynamics in a GCM, *Clim. Dyn.*, *28*, 581–597.

DeMott, P., D. Cziczo, A. Prenni, D. Murphy, S. Kreidenweis, D. Thomsom, R. Borys, and D. Rogers (2003), Measurements of the concentration and composition of nuclei for cirrus formation, *Proc. Natl. Acad. Sci. U. S. A.*, *100*(25), 14,655–14,660.

Dörnbrack, A. (1998), Turbulent mixing by breaking gravity waves, *J. Fluid Mech.*, *375*, 113–141.

Fusina, F., P. Spichtinger, and U. Lohmann (2007), The impact of ice supersaturated regions and thin cirrus on radiation in the midlatitudes, *J. Geophys. Res.*, *112*, D24S14, doi:10.1029/2007JD008449.

Gayet, J.-F., F. Auriol, A. Minikin, J. Ström, M. Seifert, R. Krejci, A. Petzold, G. Febvre, and U. Schumann (2002), Quantitative measurement of the microphysical and optical properties of cirrus clouds with four different in-situ probes: Evidence of small ice crystals, *Geophys. Res. Lett.*, *2*(24), 2230, doi:10.1029/2001GL014342.

Gayet, J.-F., J. Ovarlez, V. Shcherbakov, J. Ström, U. Schumann, A. Minikin, F. Auriol, and A. Petzold (2004), Cirrus cloud microphysical and optical properties at southern and northern midlatitudes during the INCA experiment, *J. Geophys. Res.*, *109*, D20206, doi:10.1029/2004JD004803.

Haag, W., and B. Kärcher (2004), The impact of aerosols and gravity waves on cirrus clouds at midlatitudes, *J. Geophys. Res.*, *109*, D12202, doi:10.1029/2004JD004579.

Hoyle, C., B. Luo, and T. Peter (2005), The origin of high ice crystal number densities in cirrus clouds, *J. Atmos. Sci.*, *62*, 2568–2579.

Jeuken, A. B. M., P. C. Siegmund, L. C. Heijboer, J. Feichter, and L. Bengtsson (1996), On the potential of assimilating meteorological analyses in a global climate model for the purpose of model validation, *J. Geophys. Res.*, *101*, 16,939–16,950.

Kärcher, B., and U. Lohmann (2002), A parameterization of cirrus cloud formation: Homogeneous freezing of supercooled aerosols, *J. Geophys. Res.*, *107*(D2), 4010, doi:10.1029/2001JD000470.

Kärcher, B., and J. Ström (2003), The roles of dynamical variability and aerosols in cirrus cloud formation, *Atmos. Chem. Phys.*, *3*, 823–838.

Klein, S. A., and C. Jakob (1999), Validation and Sensitivities of Frontal Clouds Simulated by the ECMWF Model, *Mon. Weather Rev.*, *127*, 2514–2531.

Koop, T., B. Luo, A. Tsias, and T. Peter (2000), Water activity as the determinant for homogeneous ice nucleation in aqueous solutions, *Nature*, *406*, 611–614.

Kuo, Y. H., and Y. R. Guo (1989), Dynamic initialization using observations from a network of profilers and its impact on short range numerical weather prediction, *Mon. Weather Rev.*, *117*, 1975–1998.

Lindzen, R. (1981), Turbulence and stress due to gravity wave and tidal breakdown, *J. Geophys. Res.*, *86*, 9707–9714.

Lohmann, U., and B. Kärcher (2002), First interactive simulations of cirrus clouds formed by homogeneous freezing in the ECHAM general circulation model, *J. Geophys. Res.*, *107*(D10), 4105, doi:10.1029/2001JD000767.

Lohmann, U., P. Stier, C. Hoose, S. Ferrachat, S. Kloster, E. Roeckner, and J. Zhang (2007), Cloud microphysics and aerosol indirect effects in the global climate model ECHAM5-HAM, *Atmos. Chem. Phys.*, *7*, 3425–3446.

Lott, F., and M. Miller (1997), A new subgrid-scale orographic parameterization: Its formulation and testing, *Q. J. R. Meteorol. Soc.*, *123*, 101–127.

McFarlane, N. (1987), The effect of orographically excited gravity wave drag on the general circulation of the lower stratosphere and troposphere, *J. Atmos. Sci.*, *44*, 1775–1800.

Pruppacher, H., and J. Klett (1997), *Microphysics of Clouds and Precipitation*, 954 pp., Kluwer Acad., Dordrecht, Netherlands.

Roeckner, E., et al. (2003), The atmospheric general circulation model ECHAM5. PART I: Model description, Report 349, Max Planck Inst. for Meteorol., Hamburg, Germany.

Rossow, W., and R. Schiffer (1999), Advances in understanding clouds from ISCCP, *Bull. Am. Meteorol. Soc.*, *80*(11), 2261–2287.

Sassen, K., and G. Dodd (1989), Haze particle nucleation simulation in cirrus clouds and application for numerical and lidar studies, *J. Appl. Sci.*, *46*, 3005–3014.

Smith, R. B. (1979), The influence of mountains on the atmosphere, *Adv. Geophys.*, *21*, 87–230.

Smith, R. B., J. Doyle, Q. Jiang, and S. Smith (2007), Alpine gravity waves: Lessons from MAP regarding mountain wave generation and breaking, *Q. J. R. Meteorol. Soc.*, *133*, 917–936.

Spichtinger, P., and P. K. Smolarkiewicz (2008), Turbulence in cirrus clouds—Impact of critical layers (extended abstract), paper presented at Int. Conf. on Clouds and Precip., Cancun, Mexico.

Spichtinger, P., K. Gierens, and A. Dörnbrack (2005a), Formation of ice supersaturation by mesoscale gravity waves, *Atmos. Chem. Phys.*, *5*, 1243–1255.

Spichtinger, P., K. Gierens, and H. Wernli (2005b), A case study on the formation and evolution of ice supersaturation in the vicinity of a warm conveyor belt's outflow region, *Atmos. Chem. Phys.*, *5*, 973–987.

Uppala, S. M., et al. (2005), The ERA-40 re-analysis, *Q. J. R. Meteorol. Soc.*, *131*, 2961–3012.

Wallace, J. M., S. Tibaldi, and A. J. Simmons (1983), Reduction of systematic errors in the ECMWF model through the introduction of an envelope orography, *Q. J. R. Meteorol. Soc.*, *109*, 683–717.

Webb, M., C. Senior, S. Bony, and J.-J. Morcrette (2001), Combining ERBE and ISCCP data to assess clouds in the Hadley Centre, ECMWF and LMD atmospheric climate models, *Clim. Dyn.*, *17*, 905–922.

J.-F. Gayet, Laboratoire de Meteorologie Physique, Universite Blaise Pascal, Aubiere CEDEX, F-63177 Clermont-Ferrand, France. (J.F.Gayet@opgc.univ-bpclermont.fr)

H. Joos, U. Lohmann, and P. Spichtinger, Institute for Atmospheric and Climate Science, ETH Zurich, Universitätstr. 16, CH-8092 Zurich, Switzerland. (hanna.joos@env.ethz.ch)

A. Minikin, Institute of Atmospheric Physics, DLR, D-82234 Oberpfaffenhofen, Germany. (Andreas.Minikin@dlr.de)